Proceedings of FEDSM2008
2008 ASME Fluids Engineering Conference
August 10-14, 2008 Jacksonville, Florida USA

FEDSM2008-55190

DEVELOPING AND FULLY DEVELOPED TURBULENT FLOW IN RIBBED CHANNELS

N. D. Cardwell
Mechanical Engineering
Virginia Polytechnic Institute
and State University
Blacksburg, VA

P. P. Vlachos
Mechanical Engineering
Virginia Polytechnic Institute
and State University
Blacksburg, VA

K. A. Thole
Mechanical and Nuclear Engineering
Pennsylvania State University
University Park, PA

ABSTRACT

Modern turbomachines operate at combustion temperatures well beyond the incipient melting point of the turbine's metal components. Cooling channels within turbine airfoils directly affect component lifecycle in addition to influencing almost all aspects of the overall engine design. However, many aspects regarding flow structure and vortex dynamics within these cooling channels are still unknown.

In this study, high fidelity Time Resolved Digital Particle Image Velocimetry (TRDPIV) was used to investigate a ribbed cooling channel. The design consisted of a square channel having square transverse ribs which were staggered on both the top and bottom walls. Rib spacing was matched to the channel height and the rib to channel height ratio was kept constant at 0.13. The Reynolds number range investigated was between 2,500 and 20,000. Flow field measurements were performed at the entrance to and within the developed rib roughened section, corresponding to the 1st and 12th ribs.

Overall, the results indicate that large scale coherent vortical structures were generated by the presence of the front rib surface and enclosed wake region between the ribs. Higher values of vortex circulation strength were observed for Re=2,500 in addition to a more homogeneous distribution of identified coherent structures at the developed section. In addition to providing insight and feedback for a common turbine cooling design, this study also illuminates the vortex distribution for a highly turbulent and complex internal flow.

INTRODUCTION

Internal cooling channels are typically used within a gas turbine to convect heat from the turbine blades and vanes. Relatively colder, high pressure air is bled from the compressor, bypassed around the combustor, and then circulated through the cooling channels within the turbine. These cooling channels are often designed with turbulence promoters that serve to increase convective heat transfer between the internal metal surfaces and coolant flow. Within a gas turbine, the most commonly utilized turbulence promoter is the transverse rib. Arrays of ribs are placed within the cooling channels which augments the turbulent heat transfer between the metal surfaces and coolant. Internal channels with arrays of ribs are often referred to as rib roughened channels. This relatively simple internal cooling geometry has been the subject of numerous studies owing to its effectiveness in increasing convective heat transfer with only minor increases in pressure drop versus a smooth channel. In addition to cooling effectiveness, the presence of the ribs produces a flow field governed by separated flow and recirculation in the near-rib region and vortex shedding into a highly turbulent core flow.

One of the earliest studies of rib roughened turbulent boundary layer flow was performed by Perry et al. [1]. They showed that the effective roughness of spanwise grooves could be characterized by either the roughness height, k, or the boundary layer thickness, d. D-type roughness elements, where rib pitch was less than 3 times the rib height, were characterized by fully separated flow over the rib surfaces in addition to a sustained inter-rib vortex. K-type roughness was described by a sufficiently large rib pitch such that the separated flow over the initial rib became fully reattached at the wall before encountering the next rib. The review by Jimenez [2], discusses the state-of-the-art for both d-type and k-type roughness. A more recent computation study by Cui et al [3] using a Large Eddy Simulation (LES) further explored the effect of rib spacing. Their domain consisted of periodically bounded channel flow with a single rib roughened wall. For d-type roughness, the mean outer flow was observed "riding" over the roughness elements with a separated vortex contained between each rib pair. With the larger separated k-type roughness, reattachment occurred between subsequent ribs and large vortices were identified within the core flow through qualitative observations of the instantaneous velocity vector fields. For an intermediate roughness type, where the

Copyright © 2008 by ASME

rib pitch was equal to 4 times the rib height, the extent of the mean separation cavity was roughly equivalent to the rib pitch. However, the core flow was significantly affected by vortex shedding from the semi-separated inter-rib cavity. An experimental study by Wang et al [4] regarding a single wall roughened channel supported the results of Cui et al. [3] for k-type roughness elements.

Another study on intermediate and k-type roughness was performed by Rau et al. [5]. They analyzed the effect of rib presence on the wall heat transfer. They found that average wall heat transfer was higher for the k-type roughness elements, owing to the impingement on the upstream rib face which occurred after reattachment of the separated shear layer. Ultimately, these studies are limited in practical application as the majority of cooling channels have roughness elements on both the top and bottom walls, which are commonly referred to as fully roughened channels.

Only a limited number of experimental studies have sought to resolve the flow field of a fully roughened channel. Using laser Doppler velocimetry (LDV) Liou et al. [6,7] studied the main and secondary flows in a fully roughened rectangular channel with vertically aligned k-type rectangular roughness elements. Their research showed that the separated shear layer growth and reattachment length were markedly different than for a geometrically similar backward facing step. Graham et al. [8], for a fully roughened channel with aligned ribs, evaluated the effect of rib height for a fixed rib pitch. Using LDV and pressure drop measurements, Graham et al. [8] concluded that increasing rib height resulted in a larger recirculation region between successive ribs thus explaining the trend of decreasing inter-rib heat transfer as observed by other researchers. Graham et al. [8] also observed that the required development length for a k-type fully roughened channel was approximately 10 rib pitches. This development length was larger than values previously reported by other researchers, which were derived as the channel friction factor became constant at an approximate value of 4 rib pitches. The study by Graham et al. [8] showed that, while average friction factor does become constant after 4 ribs, the center channel averaged velocity does not become developed until after the 10^{th} rib. Despite a number of experimental studies on aligned rib roughness elements, few studies have focused on the effects of staggered rib elements.

Numerous computational studies have been performed on rib roughened channel geometries, such as those by Wahab and Tafti [9], Cui et al. [3], and Sewall and Tafti [10]. A thorough review of the contributions and difficulties in simulating roughened channels was provided by Patel [11]. Recent numerical studies are beginning to rely on LES and Direct Numerical Simulations (DNS) to more accurately resolve the flow field than previous studies utilizing the Reynolds Averaged Navier-Stokes equations (RANS). However, the lack of computational resources limits LES and DNS to periodic boundary approximations, coarse grids, and lower Reynolds numbers. Lastly, there is a lack of high resolution experimental data to further validate the computationally derived rib roughened channel flow field.

NOMENCLATURE

C	circulation strength
d	diameter
D_h	hydraulic diameter
e	rib height
h	channel height
p	rib pitch
Re	Reynolds number $Re = U_b D_h / \nu$
U	velocity

Greek

ν	kinematic viscosity

Subscripts

b	bulk property

EXPERIMENTAL FACILITIES AND METHODOLOGY

This section describes the selection, generation, and quantification of a rib roughened channel flow field relevant to a gas turbine internal cooling channel.

Staggered Rib Channel Geometry

The rib roughened channel used for this study was based on an actual internal cooling channel within a turbine vane. An experimental setup was constructed to simulate a turbine cooling channel, as shown in Figure 1. The experimental coolant channel has both a smooth and rib roughened section. A length of $12D_h$ was chosen for smooth wall inlet section to generate fully developed flow to the rib roughened channel section for the range of flowrates tested. A summary of relevant channel dimensions are given in Figure 2 and Table 1 as well as a comparison between the engine and scaled up experimental geometry. Transverse spanwise ribs were placed 90° to the main channel flow on both the upper and lower walls. As shown in Figure 2, the opposite wall ribs were symmetrically staggered with respect to each other. This type of staggered rib geometry was chosen as it matches with what is commonly seen within the engine. The coordinate system, shown in Figure 2, was defined based on the channel

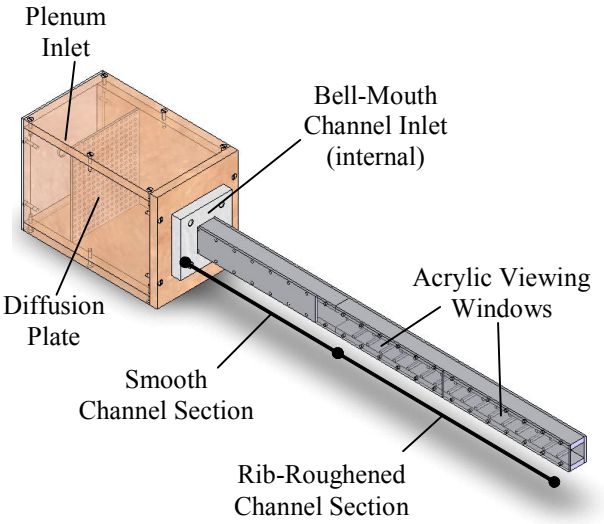

Figure 1. Illustration of the rib-channel experimental setup.

Copyright © 2008 by ASME

Table 1. Rib and Channel Geometric Parameters

	PW4168A 2nd Vane	6X Experimental Model
Height (h)	~0.6cm	3.8cm
Aspect Ratio	0.5-2	1
e/D_h	0.1	0.12
p/e	5 - 10	8
p/D_h	~1	1
rib angle	45°-90°	90°
Re	10k-100k	2.5k, 10k, 20k

centerline and upstream face of the 1st rib on the top wall. An experimental channel scale of 6X was chosen to provide a good tradeoff between increasing measurement resolution and flowrate limitations of the coolant flow supply. Regarding the previously discussed studies, the experimental rib pitch to channel height ratio corresponded to k-type roughness.

Test Facility

The experimental test setup used to analyze the staggered rib channel geometry is shown in Figure 3. High pressure, room temperature air was supplied as coolant to the test channel. This air was distributed to the lab by an auxiliary compressor facility at approximately 550 kPa. A gate valve, situated far upstream of the plenum inlet, was used to control and regulate coolant flowrate. Total coolant flowrate to the channel was measured upstream of the plenum inlet by measuring pressure drop across a laminar flow element (LFE). The LFE had a maximum flowrate capacity of 1.2 m^3/s and a measured flowrate uncertainty of ±0.5%. Flowrate requirements for the channel ranged from 0.1-0.7 m^3/s. A Validyne DP-103 differential pressure transducer was used to measure the pressure drop across the LFE. The measured range of pressure drop was 150–1196 Pa with a transducer measurement accuracy of ±0.25% of the 2216 Pa full scale. After passing through the LFE, the flow entered a 40:1 area ratio plenum compared to the channel flow area. Within the

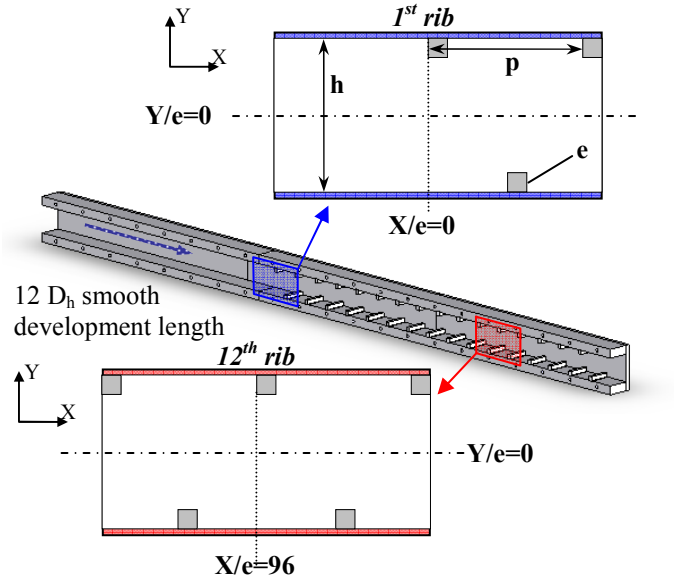

Figure 2. Section view of the rib channel illustrating the inlet and fully developed measurement planes.

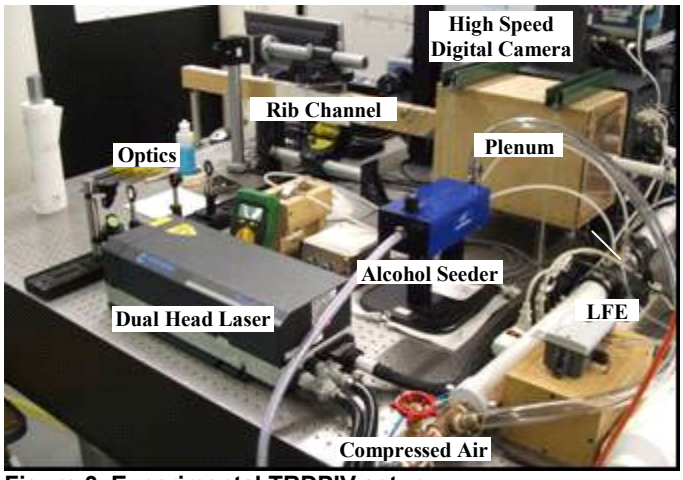

Figure 3. Experimental TRDPIV setup.

plenum the coolant flow passes through a round-hole diffusion plate having a closed to open area ratio of 4:1. After passing through the diffusion plate, the coolant entered the channel section through a bell-mouth inlet to assure a smooth and uniform inlet flow. Clear acrylic was used to construct the channel, thus providing the necessary optical and laser access required to investigate the flow field using Time Resolved Digital Particle Image Velocimetry (TRDPIV).

Flow field Measurement Method - TRDPIV

TRDPIV is an advanced experimental technique providing temporal-spatially resolved, noninvasive, high fidelity velocity field measurements. The major components of any TRDPIV system include: fluid tracing particles, a high power pulsing laser, optics, and a high speed digital camera.

For the presented study, seeding of the flow with fluid tracing particles was accomplished using a LaVision alcohol based liquid atomizer, which produced approximately 1μm diameter particles. The Stokes number of these particles within the channel was much less than 1, satisfying the criterion for a flow tracer. As seen in Figure 3, the alcohol flow tracers were injected upstream of the LFE.

Another critical element of the TRDPIV system was a high power pulsing laser, which was used to illuminate the flow tracers above the level of background light. The current study utilized a 20W New Wave dual-head Pegasus laser, having a maximum double pulse frequency of 10kHz. The laser beam was manipulated into a very thin (<1mm) two-dimensional plane, through the use of lenses and mirrors, and then passed through the channel's lower wall. Referring to Figure 2, two regions of interest were defined within the ribbed channel section. The inlet and developed regions of interest were centered on the 1st and 12th rib, respectively. The regions of interest were $2.1D_h$ streamwise by $1D_h$ spanwise.

The last major component for a TRDPIV system was a high speed digital camera. Placed normal to the laser sheet, the camera recorded images of the fluid tracers at precisely controlled time intervals. Using correlation techniques, the fluid motion may then be computed directly from the inter-frame flow tracer displacement. A Photron Ultima APX-RS high speed digital camera, having a maximum frame capture rate of 6000fps at megapixel resolution, was used for the current study. With an 8GB buffer, the Photron was able to

Copyright © 2008 by ASME

capture ~12000 frames per test. Camera resolution was set to 1024x464 pixels resulting in a spatial resolution of 84.7μm/pixel within the regions of interest.

Additional equipment employed in the study included a central data acquisition PC and Integrated Design Tools timing hub, which were used to control the laser and camera sampling frequencies. A Tektronics TDS 2014 oscilloscope was also used to monitor synchronization of the camera and laser timing signals.

TRDPIV Analysis – Generalized Cross Correlation and Robust Phase Correlation

The most common method of analyzing DPIV images employs a standard Cross Correlation technique (SCC). The SCC utilizes Fast Fourier Transform (FFT) based correlation to measure particle displacement between image pairs [12, 13,14]. Herein we use a new technique, termed Robust Phase Correlation (RPC) by Eckstein and Vlachos [15] which improves upon the SCC by employing optimum spectral filtering based on a generalized cross-correlation. The method has been shown to increase measurement accuracy while reducing peak-locking. Supporting the results of Eckstein and Vlachos [15], significant improvements in valid vector detection and measurement accuracy were observed for the present rib channel experiment when using the RPC technique versus the SCC technique (data not shown). Therefore all processing was performed with the new RPC using the parameters in Table 2. It is important to note that, for the range of Reynolds numbers tested, the TRDPIV spatial resolution was beyond what has been reported for similar rib roughened channel geometries.

Proper Orthogonal Decomposition Analysis

Proper Orthogonal Decomposition (POD) was originally proposed by Lumley [16,17] as a tool for analysis of turbulent flows and identification of coherent structures. In the present study, POD was used to analyze the energy content and dimension of the flow fields under consideration. A full description of this method is beyond the scope of this paper and the reader is referred to the works by Sirovich [18], Aubry et al. [19], Ball et al. [20] and Duggleby et al. [21] for further information on the application of POD to turbulent flows.

For the current study, a POD expansion was performed on 750 time-resolved flow samples for each Reynolds number at both the inlet and developed regions of interest. Comparisons of the number of modes required to recover 99% of the total energy content were made in addition to reconstructing the 99% energy flow field minus the first eigenmode. The removal of the first mode can be compared to Galilean decomposition [22] which is a commonly used for visualizing coherent structures in the flow.

Table 2. DPIV Parameters (pixels)

	1st Pass - RPC 2nd Pass - RPC
1st pass correlation window	64x32 (pixels)
2nd pass correlation window	32x16 (pixels)
grid spacing	4x4 (pixels)
measurement overlap	50% x 25%
number of vectors	241x111
flow samples per test	6000
flow sampling frequency	1500 Hz

Vortex Identification – Delta Criterion

Significant research has been performed on the identification and classification of a coherent structure in a turbulent flow field [23,24,25]. The method chosen for the current study was the critical point method, often referred to as the delta-criterion method, proposed by Chong et al. [24]. In short, this method defines a coherent structure as one that has a closed streamline, which is identified from the velocity gradient tensor as a region of only complex eigenvalues. It is important to note that the delta-criterion is a Galilean invariant method, meaning that it does not require a moving reference frame to identify coherent structures in the flow. Removal of the 1st eigenmode aided in the visual identification of vortical elements during data processing, facilitating the adjustment of thresholding parameters which limited the number of false vortex identifications. In addition, removing the energy content above 99% effectively filtered the flow field of high frequency information which could compromise the effectiveness of the delta-criterion method.

DISCUSSION OF RESULTS

Six tests were performed using the previously described experimental rib channel setup and TRDPIV system including Reynolds numbers of 2,500, 10,000, and 20,000 for both the inlet and developed region of interest. The selected Reynolds numbers span the range of transitioning to fully turbulent smooth channel flow.

The experimental results are broken into three sections: mean flow field analysis, POD analysis, and vortex identification. All mean flow results are averaged over 6000 flow samples. Regarding the POD and vortex identification, computational limitations restricted the analysis to 750 flow samples. To assure that the smaller sample size did not bias the results, an evaluation of the first and last set of 750 flow samples was performed. Comparisons between the two sample groups, within a given data set, showed no appreciable differences in POD reconstruction or energy distribution.

Mean Flow field Analysis

Spanwise profiles of the mean and fluctuating velocity components are shown in Figure 4a-b, corresponding to inlet and developed regions. This data confirms that the channel flow was fully developed by the 12 rib, or X/e=96.

Observations of the streamwise velocity profile in Figure 4a show that the flow entering the ribbed section, X/e=0, was similar for Re=10,000 and 20,000. A slight deviation in the inlet velocity profile was observed for Re=2,500. This small difference was attributed to slower transitional boundary layer growth within the smooth inlet section for Re=2,500 when compared to the fully turbulent boundary layer growth at Re=10,000 and 20,000. As shown in Figure 4b, the presence of the 1st rib at X/e=0 causes a strong spike in velocity fluctuations just above the rib at Y/e=3 for all Reynolds numbers. Compared to the smooth bottom wall, the presence

Copyright © 2008 by ASME

of the first rib increased peak U_{RMS} values from U_{RMS}/U_b~=0.16 at the bottom wall to U_{RMS}/U_b =0.27 at the top rib. At X/e=0, the increase in U_{RMS} caused by the 1st rib did not extend significantly into the core flow, as observed by the symmetric profiles of U_{RMS} from Y/e=2 to -2. At X/e=96 and 104, the profiles of U/U_b and U_{RMS}/U_b were mostly symmetric about Y/e=0 with the effects of the ribs on the velocity profiles extending into the core flow, further indicating that the flow was developed by this location.

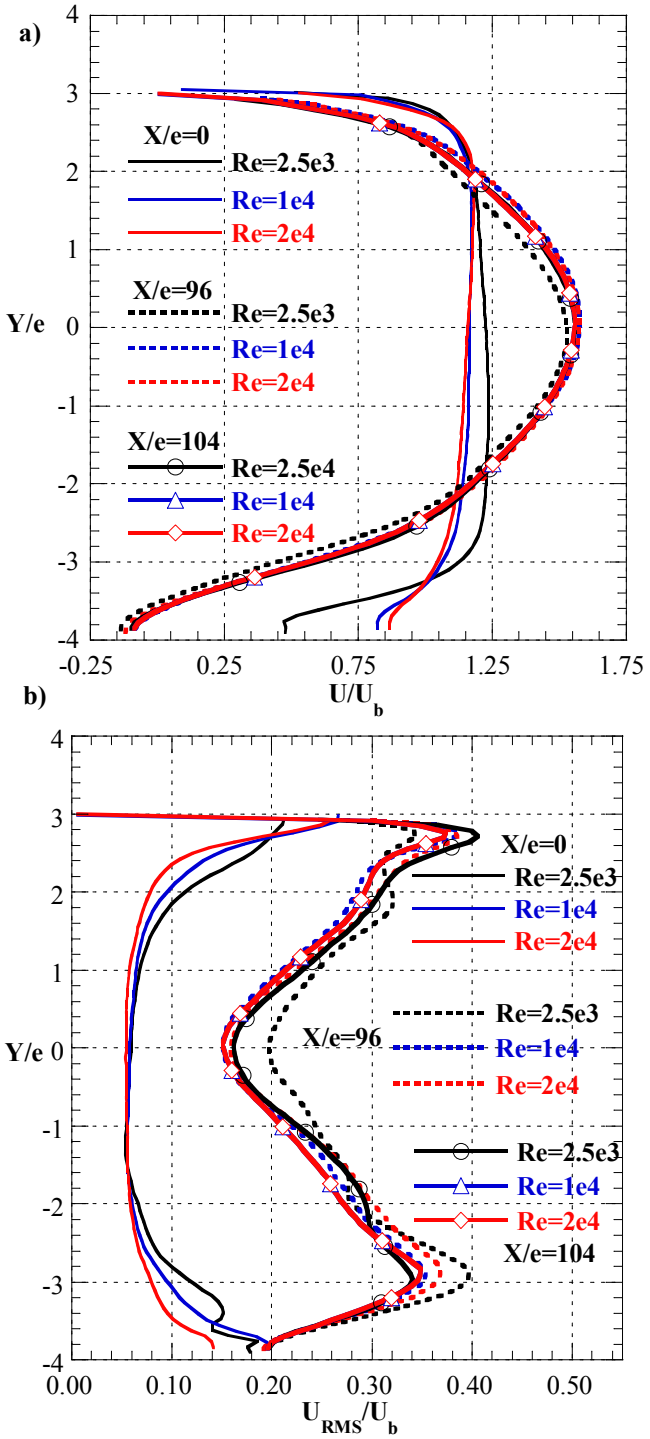

Figure 4. a) Mean b) and RMS velocities at the inlet and developed region.

As discussed earlier, the study by Graham et al. [8] reported a required development length of 10 rib pitches for a rib roughened channel flow having aligned ribs on both the top and bottom walls at Re=20,000. The velocity profiles in Figure 4a and 4b confirm that this criterion also holds true for a staggered rib configuration at the tested Reynolds numbers.

Contour plots of normalized turbulent kinetic energy (TKE) overlaid with mean velocity stream traces are shown in Figures 5 and 6 for the inlet region and Figures 7 and 8 for the developed region. Shown in Figure 5a and 6a, the mean approaching flow to the first rib splits at Y/e~=3.3 with the near wall flow rolling into a small recirculation region centered at Y/e=3.6, X/e=-0.6. The rest of the approaching flow fully separates between the 1st and 2nd ribs with a small recirculating region upstream of the second rib at Y/e=7.6, X/e=3.4. At Re=10,000 and 20,000, no appreciable differences in the velocity flow field or turbulent kinetic energy were observed at the 1st rib, as shown in Figures 5b-c and 6b-c. The recirculating region upstream of the 1st rib was no longer resolved as with Re=2,500. Similarly to turbulent flow over a cylinder, the wake region behind the rib was closing more rapidly at Re=10,000 and 20,000, a result of the increased levels of TKE in the 1st rib shear layer. At higher Reynolds numbers, a large recirculating region was observed behind the 1st rib from X/e=1 to 5 and Y/e=2.4 to 4. In addition, the recirculating region upstream of the 2nd rib was no longer sufficiently resolved and was most likely very small if present at all. At Re=2,500, the peak TKE slowly increases to a maximum value just upstream of the 2nd rib, X/e=8. For the higher Reynolds number flows, the TKE spikes occurs much earlier at X/e~=2. Value of TKE then spread outward toward the wall and core flow as the flow progresses downstream between the ribs, X/e=2 to 7.

In contrast to the Reynolds number dependence at the inlet, no appreciable differences were observed at the developed section for all three Reynolds numbers. Shown in Figure 7a and 8a, the near-rib developed velocity field at Re=2,500 closely resembled the inlet results in Figure 6b-c for the higher Reynolds numbers. The small recirculating region upstream of the rib, at X/e=95.5 and Y/e=3.7, was still present but appeared diminished in size and strength.

In addition, the flow between the ribs was no longer fully separated. A large recirculating region downstream of the 12th rib, X/e=97 to 101.2 and Y/e=2.4 to 4, was observed in addition to a smaller counter-rotating recirculation region centered at X/e=97.4 and Y/e=3.6. As stated previously, the flow field description for Re=2,500 also correctly portrays the higher Reynolds number tests, as shown in Figures 7 and 8.

Copyright © 2008 by ASME

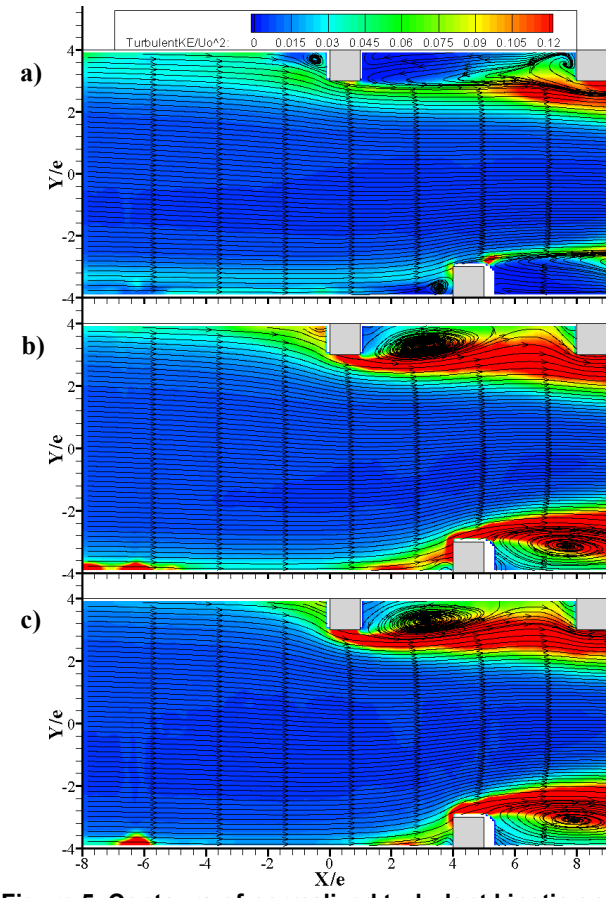

Figure 5. Contours of normalized turbulent kinetic energy overlaid with mean velocity streamtraces for a) Re=2,500, b) Re=10,000, c) Re=20,000 at the inlet section.

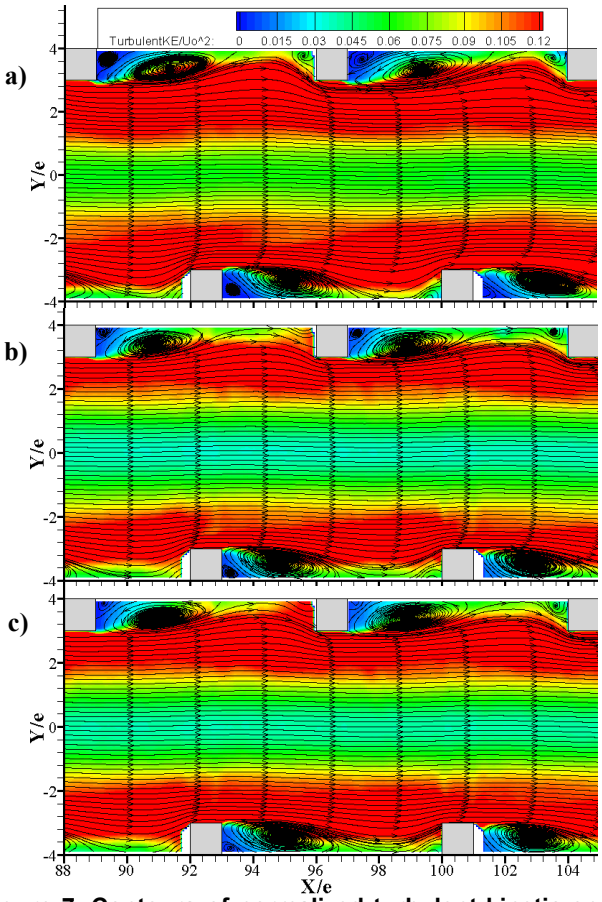

Figure 7. Contours of normalized turbulent kinetic energy overlaid with mean velocity streamtraces for a) Re=2,500, b) Re=10,000, c) Re=20,000 at the developed section.

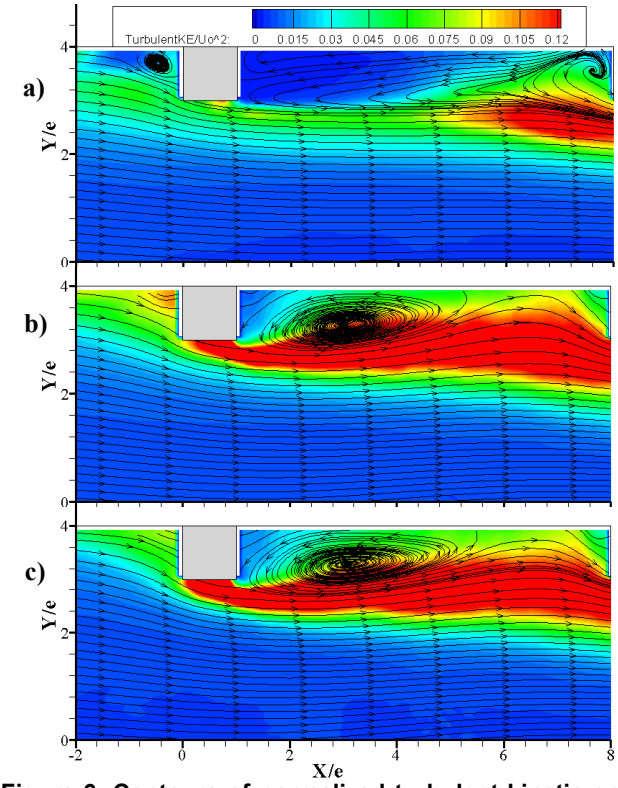

Figure 6. Contours of normalized turbulent kinetic energy overlaid with mean velocity streamtraces for a) Re=2,500, b) Re=10,000, c) Re=20,000 at the inlet section.

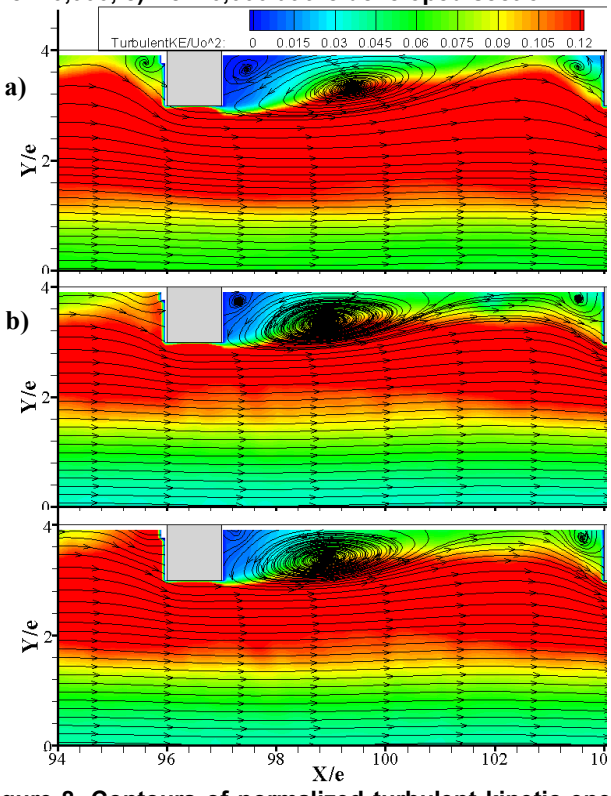

Figure 8. Contours of normalized turbulent kinetic energy overlaid with mean velocity streamtraces for a) Re=2,500, b) Re=10,000, c) Re=20,000 at the developed section.

Copyright © 2008 by ASME

Analysis of Energy Spectrum and POD reconstruction

The results of the POD decomposition are shown in Figures 9 and 10 and serve to illustrate the relative distribution of energy between the different test cases as well as the total number of modes used to reconstruct the flow field for vortex identification. For Re=2,500 at the inlet region, the dimension of the system was very low with the 99% of the energy content in the first four modes. The dimension of the higher Reynolds number flow fields were comparable and further confirms that the channel flowfield at Re=10,000 and Re=20,000 was very similar. It is important to note that there were differences in the modal energy distribution between Re=10,000 and 20,000, suggesting that the mean flow analysis was insufficient to distinguish differences in the flowfield at higher Reynolds numbers. A more thorough analysis of the individual eigenmodes is needed to explore potential differences in high Reynolds number ribbed channel flows. As such, this type of analysis was beyond the scope of this study and was reserved for another work.

As discussed in the method section, reconstruction of the flow field was performed after removing the 1st eigenmode. Contour plots of normalized vorticity overlaid with velocity vectors, shown in Figure 11, illustrate the effectiveness of a 1st eigenmode subtraction for visual identification of coherent structures within the flow.

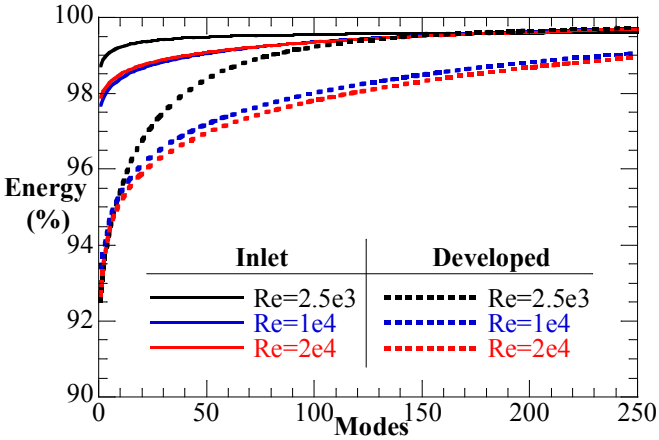

Figure 9. Cumulative energy content plot obtained through POD analysis for Re-2,500, 10,000, and 20,000 at both the inlet and fully developed section.

Results of Vortex Identification

The delta-criterion method was applied to 750 flow samples at both the inlet and developed sections for all three Reynolds numbers. Figure 12 and 13 illustrate the population of coherent structures at the inlet section for all Reynolds numbers. The same information associated with the developed section is presented in Figures 14 and 15. All scatter plots of coherent structures, Figures 12 and 14, are colored by the circulation strength of the identified vortical element. Two-dimensional histograms of identified structures are also shown in Figures 13 and 15.

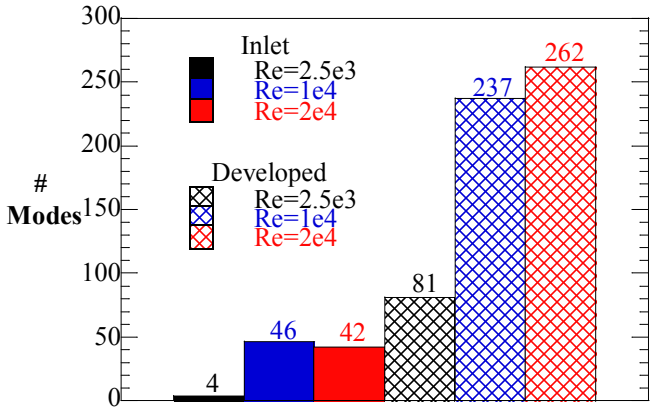

Figure 10. Comparison of the number of modes required to recover 99% energy content for Re-2,500, 10,000, and 20,000 at both the inlet and fully developed section.

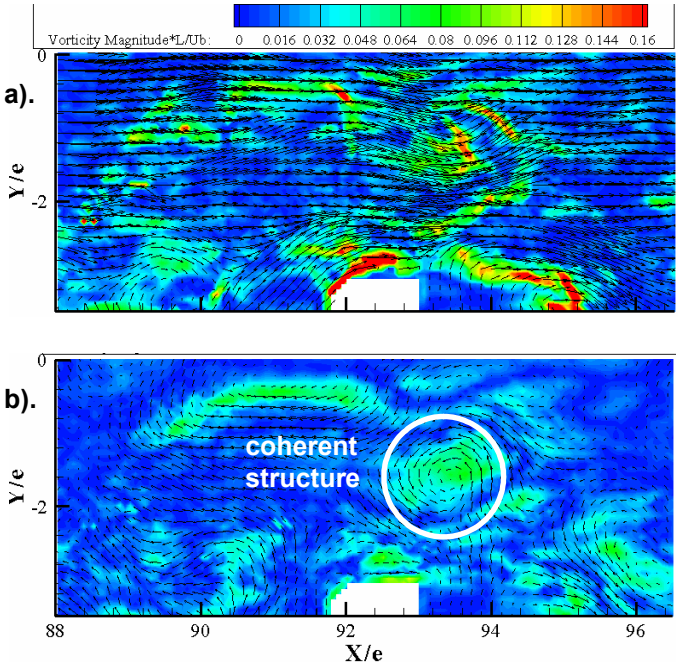

Figure 11. Contours of vorticity overlaid with velocity for a). the PIV processed flowfield b) 1st mode removed POD reconstructed flow field at Re=10,000.

For Re=2,500 at the inlet, Figure 12a shows very few identified coherent structures, with the majority located at X/e=5 to 9. This result did not hold for Re=10,000 and 20,000, as shown in Figure 12b-c. Numerous smaller, lower strength coherent structures were identified in the top and bottom wall approaching flow in addition to a plume of higher strength coherent structures identified in the wake region between the 1st and 2nd ribs. Two dimensional histograms of identified coherent structures are shown in Figure 13, showing that the population of vortices for Re=10,000 and 20,000 were also very similar Two bands of identified coherent structures were observed downstream of the 1st rib. The top band, at Y/e~=2.5, corresponds to the separated shear layer which was identified as the region of peak TKE of the mean averaged flow field. Identified coherent structures in this region likely

Copyright © 2008 by ASME

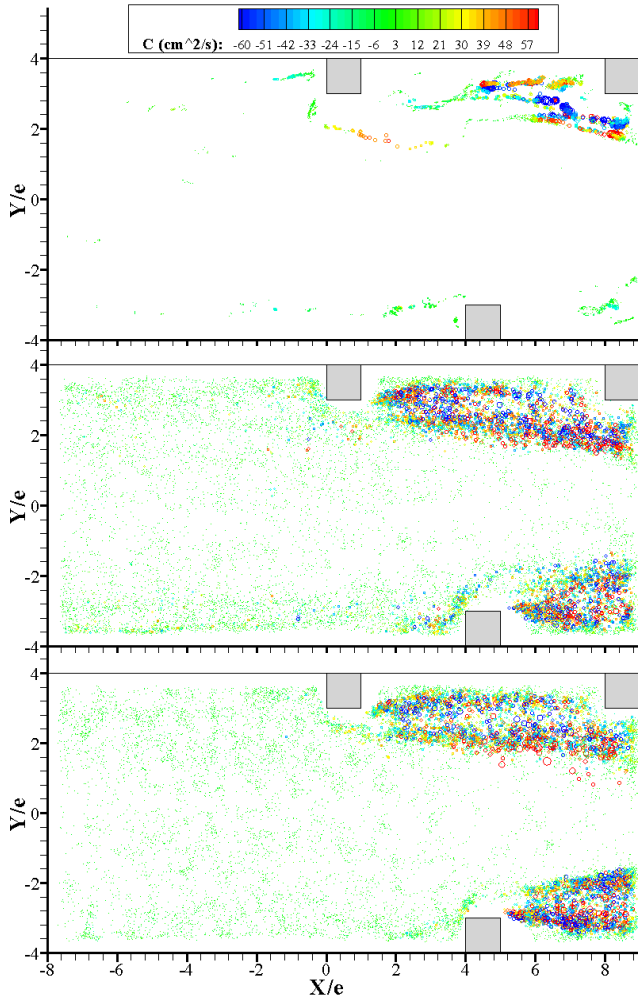

Figure 12. Identified coherent structures at the inlet for 750 flow samples at Re a) 2,500, b) 10,000, c) 20,000.

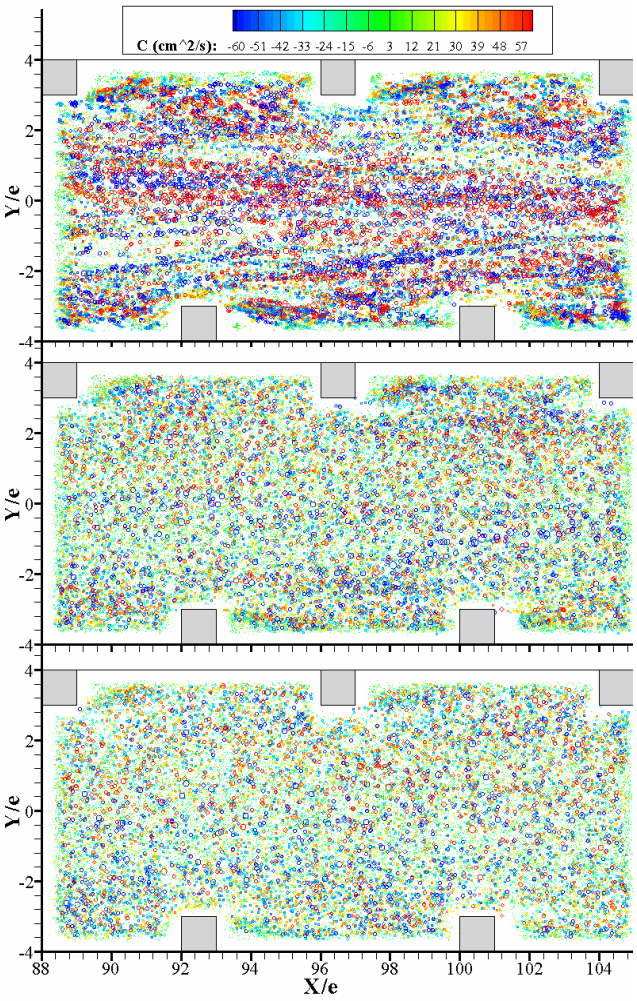

Figure 14. Identified coherent structures at the developed for 750 flow samples at Re a) 2,500, b) 10,000, c) 20,000.

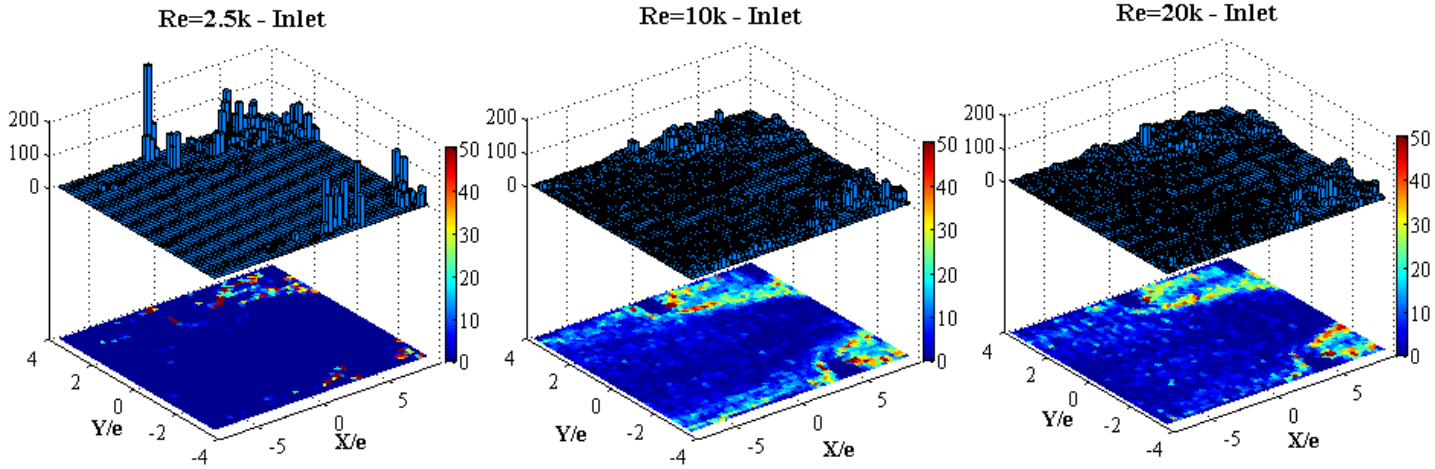

Figure 13. Vortex identification histograms for the inlet region at Re=2,500, 10,000, and 20,000.

Copyright © 2008 by ASME

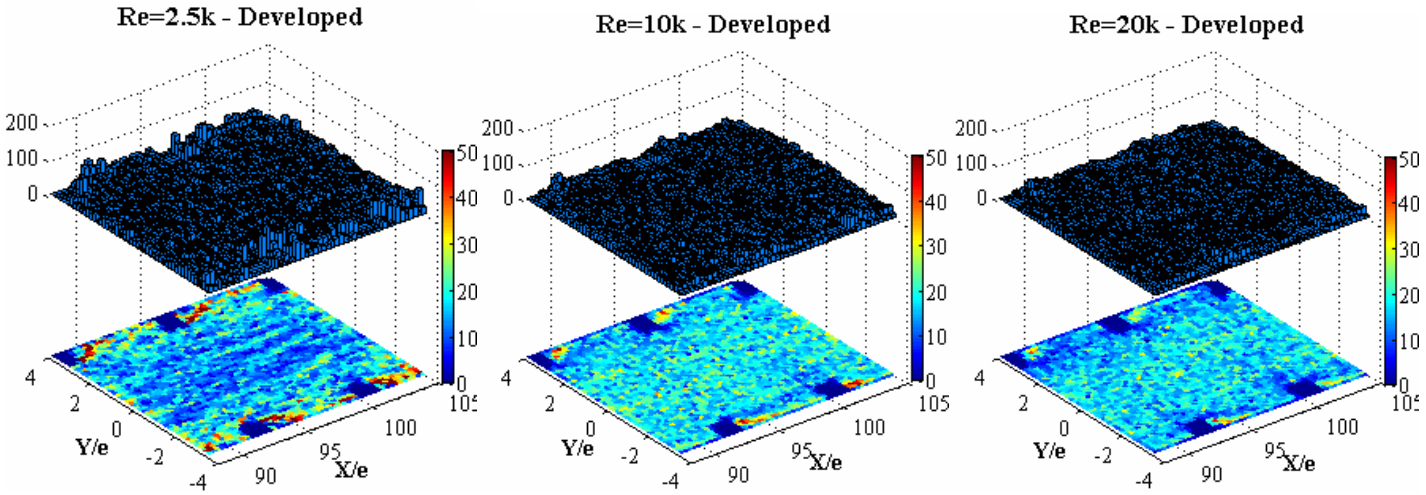

Figure 15. Vortex identification histograms for the developed region at Re=2,500, 10,000, and 20,000.

were generated by separation off the front rib corner. The lower band situated closer to the wall and downstream rib surface corresponded to the recirculating region bounded by the separated wake region identified in the mean analysis.

As shown in Figures 14 and 15, the population of vortices in the developed section was more spatially homogeneous, which was especially true for Re=10,000 and 20,000. However, for Re=2,500, the number of coherent structures identified in the recirculating region behind each rib was higher than at Re=10,000 and 20,000. For the Re=2,500, the average circulation strength of the identified coherent structures was 32 cm^2/s, which was ~40% higher than the average circulation strength of 23.8 cm^2/s and 23.4 cm^2/s observed at Re=10,000 and 20,000, respectively. It was likely that the presence of higher strength coherent structures at Re=2,500 resulted from a reduced level of vortex stretching and dissipation than was present at Re=10,000 and 20,000.

CONCLUSIONS

The presented study examined the inlet and developed flow field of a staggered rib roughened channel with applications to the design of gas turbine cooling channels. In addition to presenting mean averaged flowfield information, the results from a POD and vortex identification analysis were also presented.

From observations of the mean averaged flowfield, the previously defined inlet development length of $12D_h$ for aligned cooling channels was verified for a staggered rib array. The effect of varying Reynolds number was studied at both the inlet and developed channel regions. At the inlet, distinct differences were observed for transitionally turbulent flow, Re=2,500, and fully turbulent flow, Re=10,000 and 20,000. The primary difference was that, for Re=2,500, the separated flow over the 1st rib surface remained separated over the inter-rib cavity. At higher Reynolds numbers, the separated shear layer closed more quickly forming a recirculation region behind the rib. Once the flow became fully developed, this Reynolds number dependence was no longer apparent in the mean averaged flowfield. Mean averaged plots of TKE and velocity streamlines showed the different flows to be similar. This similarity resulted from the presence of successive rib surfaces which transitioned the flow at Re=2,500 to fully turbulent.

Results from the POD analysis confirmed that the inlet flow at Re=2,500 was mostly steady with some fluctuating behavior, as evidenced by the low number of modes required to reconstruct the flow field. However, the number of modes required to reconstruct the low Reynolds number flow field at the developed region increased significantly and was closer to the values for higher Reynolds numbers, indicating that the flow had transitioned to being fully turbulent.

Identification of coherent structures at the inlet identified two distinct bands of vortices. A higher population was observed in the separated shear layer and within the recirculating region behind the rib. The effect of vortex shedding from successive ribs was observed by the spatially homogeneous population of vortices observed at all Reynolds numbers within the developed region. Interestingly, the average circulation strength of identified coherent structures was significantly higher for Re=2,500. From a turbine heat transfer standpoint, the presence of stronger coherent structures within the flow should increase wall heat transfer levels. An ideal cooling channel design would allow for higher Reynolds number flows while adjusting rib height and pitch to maximize vortex shedding and turbulent energy transport between the inter-rib region and the core flow.

REFERENCES

1 Perry, A.E., Schofield, W.H., Joubert, P.N., 1969. "Rough wall turbulent boundary layers", *J. Fluid Mech*. 37, pp. 383–413.

2 Jimenez, J., 2004, "Turbulent Flows over Rough Walls," *Annual Review of Fluid Mechanics*, Vol. 36, pp. 173-196.

3 Cui, J., Patel, V.C., and Lin, C.L., 2003, "Large-eddy simulation of turbulent flow in a channel with rib roughness," *Int. J. of Heat and Fluid Flow*, Vol. 24, pp. 372-388.

4 Wang, L., Hejcik, J., and Sunden, B., 2007, "PIV Measurement of Separated Flow in a Square Channel With Streamwise Periodic Ribs on One Wall," *J. of Fluids Engineering*, Vol. 129, pp. 834-841.

Copyright © 2008 by ASME

5 Rau, G., Cakan, M., Moeller, D., and Arts, T., 1998, "The Effect of Periodic Ribs on the Local Aerodynamic and Heat Transfer Performance of a Straight Cooling Channel," *J. of Turbomachinery*, Vol. 120, pp. 368-375.
6 Liou, T.M., Chang, Y., Hwang, D.W., 1990, "Experimental and computational study of turbulent flows in a channel with two pairs of turbulent promoters in tandem," *J. Fluids Eng*. 112, pp. 302–310.
7 Liou, T.M., Hwang, J.-J., Chen, S.-H., 1993a. "Simulation and measurement of enhances turbulent heat transfer in a channel with periodic ribs on one principal wall," *Int. J. Heat Mass Transfer* Vol. 36, pp. 507–517.
8 Graham, A., Sewall, E., and Thole, K. A., "Flow field Measurement in a Ribbed Channel Relevant to Internal Turbine Blade Cooling," *ASME Paper # GT2004-53361*.
9 Wahab, S. A., Tafti, D. K., 2004, "Large Eddy Simulation of Flow and Heat Transfer in a 90 deg Ribbed Duct With Rotation: Effect of Coriolis and Centrifugal Boundary Forces," *J. of Turbomachinery*, Vol. 126, pp. 627-636.
10 Sewall, E. A., Tafti, D. K., 2006, "Large Eddy Simulation of Flow and Heat Transfer in the 180-Deg Bend Region of a Stationary Gas Turbine Blade Ribbed Internal Cooling Duct," *J. of Turbomachinery*, Vol. 128, pp. 763-771.
11 Patel, V.C, "Perspective: Flow at High Reynolds Number and Over Rough Surfaces – Achilles Heel of CFD," *J. Fluids Eng*, Vol. 120, pp. 434-444.
12 Westerweel, J., 1997, "Fundamentals of digital particle image velocimetry," *Measurement Science & Tech.*, Vol. 8, Iss. 12, pp.1379-1392.
13 Adrian, R.J., 1997, "Dynamic ranges of velocity and spatial resolution of particle image velocimetry," *Measurement Science & Tech.*, Vol. 8, Iss. 12, pp. 1393-1398.
14 Adrian, R.J., 2005, "Twenty years of particle image velocimetry," *Exp. in Fluids*, Vol. 39, Iss. 2, pp. 159-169.
15 Eckstein, A., and Vlachos, P. "A robust phase correlation DPIV processing algorithm for time resolved measurements." Proceedings of the 7th International PIV symposium, 2007, Rome, Italy.
16 Lumley, J.L., *Stochastic Tools in Turbulence*, Academic Press, New York, 1970.
17 Berkooz, G., Holmes, P., Lumley, J.L., 1993, "The Proper Orthogonal Decomposition in the Analysis of Turbulent Flows," *Annual Review of Fluid Mechanics*, Vol. 25, pp. 539-575.
18 Sirovich L (1987) Turbulence and the Dynamics of Coherent Structures I-III. *Quart App Math* 45:567-571.
19 Aubry N, Holmes P, Lumley JL, Stone E (1988) The Dynamics of Coherent Structures in the Wall Region of a Turbulent Boundary Layer*, J. Fluid Mechanics*. Vol. 192:115-173.
20 Ball, K.S., Sirovich, L., Keefe, L.R., 1991, "Dynamic Eigenfuction Decomposition of Turbulent Channel Flow," *Int. J. for Numerical Methods in Fluids*," Vol. 12, pp. 585-604.
21 A. Duggleby, K. S. Ball, M. R. Paul, and P. F. Fischer, 2007. "Dynamical Eigenfunction Decomposition of Turbulent Pipe Flow," *Journal of Turbulence*, Vol. 8, Iss. No. 43.
22 Adrian, R.J., Christensen, K.T., Liu, Z.C., 2000, "Analysis and Interpretation of Instantaneous Turbulent Velocity Fields," *Exp. in Fluids*, Vol. 29, Iss. 3, pp.275-290
23 Hunt, J.C., Wray, A.A., Moin, P., 1988, "Eddies, stream, and convergence zones in turbulent flows," *Center for Turbulence Research Report CTR-S88*, pp.193.
24 Chong, M.S., Perry, A.E., and B.J. Cantwell, 1990, "A General Classification of Three-Dimensional Flow Fields," *Physics of Fluids*, A, Vol. 2, No. 5, pp. 765-777.
25 Jeong, J., Hussain, F., 1995, "On the identification of a vortex," *J. of Fluid Mechanics.*, Vol. 285, pp.69-94.

Copyright © 2008 by ASME